Article

# Pseudospin-selective Floquet band engineering in black phosphorus

https://doi.org/10.1038/s41586-022-05610-3

Received: 13 December 2021

Accepted: 30 November 2022

Published online: 1 February 2023

Check for updates

Shaohua Zhou[1,2,8], Changhua Bao[1,2,8], Benshu Fan[1,2], Hui Zhou[3], Qixuan Gao[1,2], Haoyuan Zhong[1,2], Tianyun Lin[1,2], Hang Liu[3,4], Pu Yu[1,2,5], Peizhe Tang[6,7], Sheng Meng[3,4], Wenhui Duan[1,2,5] & Shuyun Zhou[1,2,5] ✉

Time-periodic light field has emerged as a control knob for manipulating quantum states in solid-state materials[1–3], cold atoms[4] and photonic systems[5] through hybridization with photon-dressed Floquet states[6] in the strong-coupling limit, dubbed Floquet engineering. Such interaction leads to tailored properties of quantum materials[7–11], for example, modifications of the topological properties of Dirac materials[12,13] and modulation of the optical response[14–16]. Despite extensive research interests over the past decade[3,8,17–20], there is no experimental evidence of momentum-resolved Floquet band engineering of semiconductors, which is a crucial step to extend Floquet engineering to a wide range of solid-state materials. Here, on the basis of time and angle-resolved photoemission spectroscopy measurements, we report experimental signatures of Floquet band engineering in a model semiconductor, black phosphorus. On near-resonance pumping at a photon energy of 340–440 meV, a strong band renormalization is observed near the band edges. In particular, light-induced dynamical gap opening is resolved at the resonance points, which emerges simultaneously with the Floquet sidebands. Moreover, the band renormalization shows a strong selection rule favouring pump polarization along the armchair direction, suggesting pseudospin selectivity for the Floquet band engineering as enforced by the lattice symmetry. Our work demonstrates pseudospin-selective Floquet band engineering in black phosphorus and provides important guiding principles for Floquet engineering of semiconductors.

Time-periodic light field can induce photon-dressed electronic states through virtual absorption or emission of photons, which are called Floquet states in analogy to Bloch states in spatially periodic crystals[21]. The interaction between Floquet states provides a fascinating pathway to tailor the electronic, symmetric and topological properties of quantum materials dynamically[7–11], for example, controlling the non-equilibrium topological properties of Dirac materials[13,22–25], inducing Floquet topological phase in semiconductors[3,17,19,20], as well as modulating the optical response[14–16] and tunnelling current[26].

The most fundamental physics of the Floquet band engineering lies in inducing the band hybridization between the original Bloch states and the photon-dressed Floquet sidebands. Taking a semiconductor as an example (Fig. 1a), a strong coupling between the Bloch bands ($m$, $n$ = 0 states in the framework of the Floquet theory) and the Floquet sidebands, such as $n = -1$ for the conduction band (CB) and $m = 1$ for the valence band (VB; see Fig. 1b), could lead to a dynamical gap opening at the crossing points (labelled Δ in Fig. 1c). Moreover, on near-resonance pumping, the CB edge with $n = -1$ is close to the VB edge, which could lead to a stronger interaction. Such time-dependent and momentum-dependent band renormalization can be further enriched by spin[19], valley[18] and pseudospin degrees of freedom.

Despite surging research interest over the past decade, so far direct experimental demonstration of momentum-dependent Floquet band engineering has been limited to the topological surface state of $Bi_2Se_3$ (ref. [12]), owing to its unique linear dispersions, which can couple with low-energy photons effectively. For semiconducting $WSe_2$, although the photon-dressed sidebands have been observed[27], no band renormalization has been detected yet. Whether such Floquet band engineering is indeed realistic beyond Dirac materials has remained a long-standing question. Answering this question is important, particularly considering that Floquet band engineering of a semiconductor is a critical step towards inducing transient topological states in topologically trivial materials[8]. Here, by using time- and angle-resolved photoemission spectroscopy (TrARPES) with mid-infrared (MIR) pumping (see schematic in Fig. 1d), we report experimental signatures of Floquet band engineering of a semiconducting black phosphorus on near-resonance pumping, which exhibits a strong dependence on light polarization, indicating previously unknown pseudospin selectivity.

[1]Department of Physics, Tsinghua University, Beijing, People's Republic of China. [2]State Key Laboratory of Low-Dimensional Quantum Physics, Tsinghua University, Beijing, People's Republic of China. [3]Institute of Physics, Chinese Academy of Sciences, Beijing, People's Republic of China. [4]Songshan Lake Materials Laboratory, Dongguan, People's Republic of China. [5]Frontier Science Center for Quantum Information, Beijing, People's Republic of China. [6]School of Materials Science and Engineering, Beihang University, Beijing, People's Republic of China. [7]Max Planck Institute for the Structure and Dynamics of Matter, Center for Free-Electron Laser Science, Hamburg, Germany. [8]These authors contributed equally: Shaohua Zhou and Changhua Bao. ✉e-mail: syzhou@mail.tsinghua.edu.cn

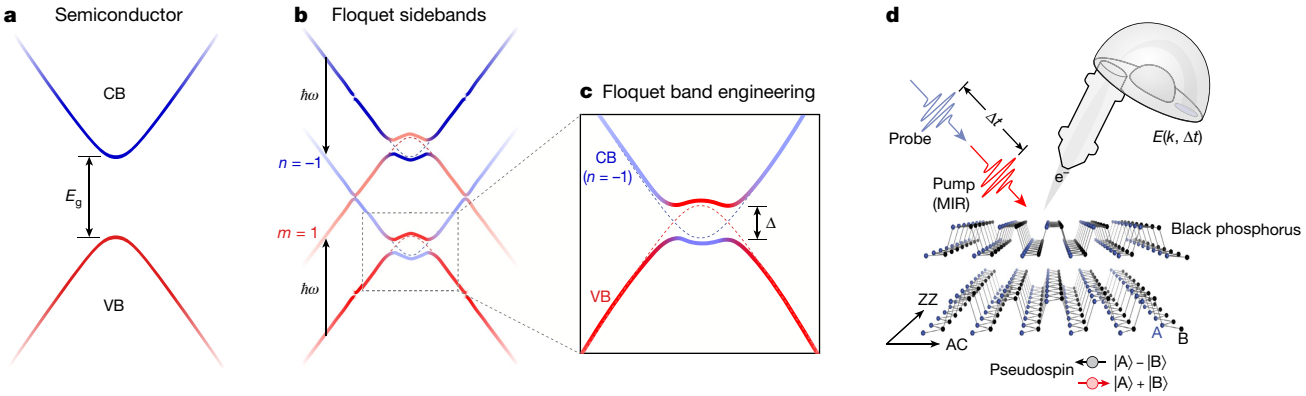


**Fig. 1 | Schematics for Floquet band engineering in semiconducting black phosphorus. a**,**b**, Schematic dispersions of a semiconductor (**a**) and corresponding Floquet sidebands (**b**). **c**, Schematic of band renormalization between the VB and Floquet sideband of the CB through Floquet band engineering. **d**, Schematic for time-resolved and angle-resolved photoemission spectroscopy with MIR pumping on black phosphorus. The inset shows the definition of pseudospin, which is a linear combination of wavefunctions on the A and B sublattices.

## Light-induced band renormalization

Black phosphorus is a direct band-gap semiconductor with anisotropic crystal structure as shown in Fig. 1d. In contrast to $WSe_2$ with a large band gap of about 1.5 eV, black phosphorus has a smaller band gap of $E_g \approx 0.33$ eV, which can be resonantly excited by MIR pump pulses, allowing for efficient Floquet band engineering. Moreover, the unit cell contains two sublattices (labelled as A and B in Fig. 1d), which can be viewed as a two-level quantum system in analogy to spin, and their linear superposition defines the pseudospin degree of freedom[28]. The coupling of pseudospin with light is strongly anisotropic. In particular, the transition from the VB edge is allowed only for light polarization along the armchair (AC) direction but not along the zigzag (ZZ) direction, resulting in anisotropic optical properties and strong photoemission intensity modulation[28–31]. Such lattice-symmetry-enforced pseudospin-selective excitation provides an opportunity to possibly enrich the Floquet band engineering physics with pseudospin selectivity.

To search for signatures of Floquet band engineering, the black phosphorus is pumped above the band gap, so that the Bloch bands and light-induced sidebands overlap and interact with each other. Figure 2a,b shows a comparison of dispersion images measured before and on pumping at 380-meV photon energy, which is slightly above the band gap. The pump polarization is along the AC direction of the sample and perpendicular to the scattering plane (*s-pol.*; see Extended Data Fig. 1 for the TrARPES experimental geometries). Because there is no electric-field component perpendicular to the sample surface to couple with the photoemission final states, laser-assisted photoemission or Volkov states[32] (photon-dressed photoemission final states) can be excluded. A striking modification of the electronic structure is observed near the VB edge on pumping. In particular, the single parabolic-like VB in the equilibrium (Fig. 2a) changes into two bands with a hat-like shaped dispersion (Fig. 2b). Such change is more pronounced by taking the second derivative of the dispersion images (Fig. 2c,d; see Methods for details), which is a common practice to visualize the angle-resolved photoemission spectroscopy (ARPES) dispersion directly. The dispersions can be extracted by fitting the energy distribution curves (EDCs) in Fig. 2e–h. A comparison of the extracted dispersions before pumping (dashed black curve in Fig. 2i) and on pumping (red and blue curves) shows that there is clearly a light-induced band renormalization in black phosphorus.

The light-induced band renormalization observed under the *s-pol.* pumping geometry can be explained by Floquet band engineering, namely, the interaction between the VB and Floquet sideband of the CB with $n = -1$ leads to a hybridization gap near the resonance points. The hybridization gap is extracted to be 79 ± 20 meV from the peak separation at the resonance points $k_5$ and $k_7$ in Fig. 2h. The band renormalization is further supported by ab initio tight-binding calculation within the Floquet theory, which shows a renormalized electronic structure for the Floquet states on pumping (Fig. 2j; see Methods for more details). We note that the observed light-induced band renormalization is in contrast to previous TrARPES studies[33–38] with pump photon energy around 1.5 eV, highlighting the importance of pumping at a previously unexplored MIR regime[1,10,11] for Floquet engineering.

## Evidences for Floquet band engineering

The Floquet band engineering is supported by the same temporal evolution of the light-induced renormalization and Floquet states. Figure 3a–d shows a series of snapshots of the transient electronic structures measured at different delay times. The sideband, which is shifted by the pump photon energy, is observed at a higher pump fluence in the *s-pol.* pump scattering (indicated by the red arrows in Fig. 3b,c), suggesting that it is contributed by pure Floquet states[32]. The temporal evolution of the Floquet sideband intensity (red symbols in Fig. 3e) shows that it exists only near time zero with a resolution-limited lifetime of 130 fs. Moreover, the light-induced band renormalization is also observed in the same timescale near time zero (indicated by the blue arrows in Fig. 3b,c) and becomes barely detectable at later delay time, for example, 100 fs (Fig. 3d). Such similar timescale for the Floquet states and light-induced band renormalization implies that the dynamical change in the electronic structure is probably induced by the Floquet band engineering.

The Floquet band engineering is further supported by the dependence on pump fluence of the renormalization gap. Figure 3f–h shows a few representative TrARPES dispersion images measured at $\Delta t = 0$ with different pump fluences, and the Floquet sideband is observed in the dispersion images (red arrow in Fig. 3g,h) and the differential image (Fig. 3i). With increasing pump fluence, the dispersion shows a stronger band renormalization with systematically enhanced hybridization gap (Fig. 3j; see Extended Data Fig. 2 for more data and analysis). The extracted hybridization gap Δ scales with the pump fluence $F_{pump}$ by $\Delta \propto F_{pump}^{0.5}$. This is in agreement with the expected scaling in the framework of Floquet engineering[8] as demonstrated in $Bi_2Se_3$ (ref. [32]), thereby providing further support for the Floquet band engineering of black phosphorus.

The light-induced renormalization is observed at resonance points at which the VB overlaps with the CB with $n = -1$, which also correspond to where direct optical transition from VB to CB occurs. We note that photoexcited holes left in the VB, that is, depleted charges before intraband scattering or electron thermalization sets in, could lead to suppression of intensity at the resonance points, which apparently behaves

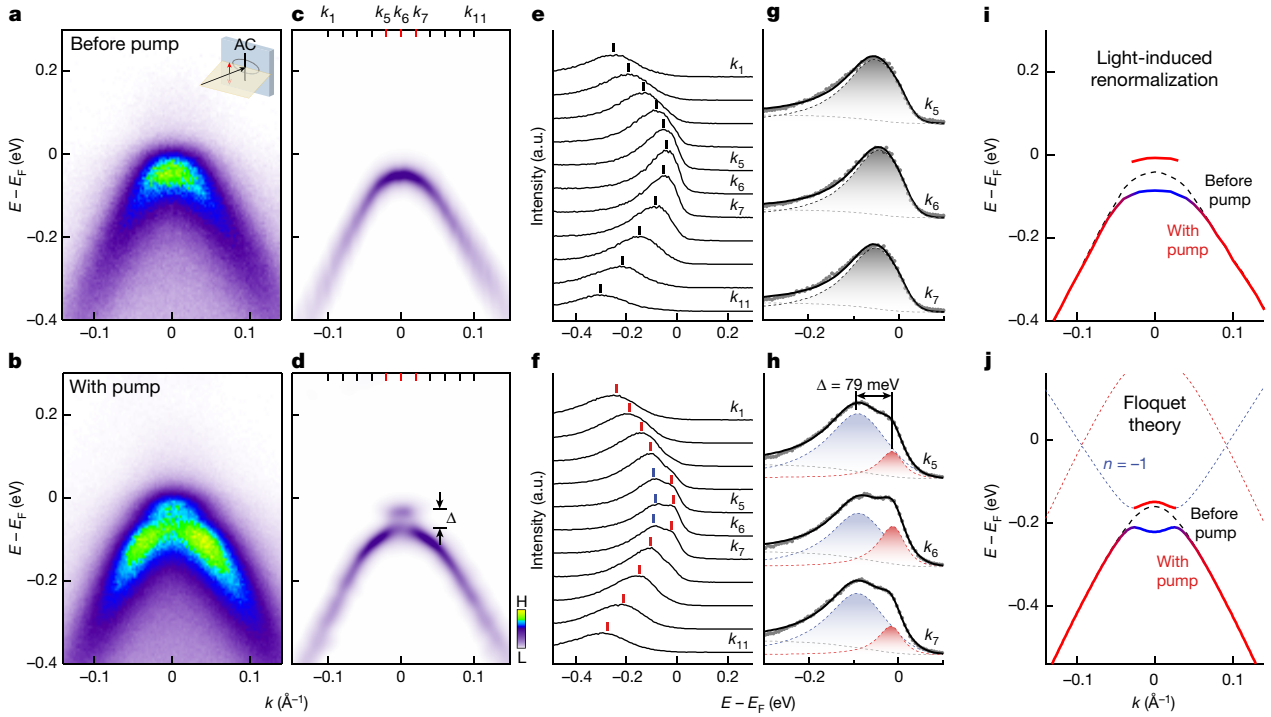


**Fig. 2 | Observation of light-induced band renormalization. a**–**d**, TrARPES dispersion images measured along the AC direction at $\Delta t = -1$ ps (**a**) and $\Delta t = 0$ (**b**), and the corresponding second-derivative images (**c**,**d**). The pump polarization is along the AC direction and perpendicular to the scattering plane (*s-pol.*), as shown in the inset in **a**. The pump photon energy is 380 meV and the pump fluence is 0.7 mJ cm$^{-2}$. **e**,**f**, EDCs for data shown in **a** and **b** at momentum points marked by the tick marks in **c** and **d**. Red and blue tick marks are the corresponding peak positions. **g**,**h**, Fitting of EDCs at resonance points ($k_5$ and $k_7$) and Γ ($k_6$) with Lorentzian peaks multiplied by the Fermi–Dirac function plus a Shirley background. **i**, Extracted dispersions before pump (dashed black curve) and with pump (red and blue curves). **j**, Calculated VB before pump (dashed black curve) and Floquet band structures (blue and red curves) with pump from the ab initio tight-binding calculations within the Floquet theory to compare with **i**.

similar to gap opening. To test this alternative explanation, we have intentionally doped the black phosphorus sample to fill the CB, so that direct optical transition is blocked on near-resonance pumping (see schematic illustration in Fig. 3k). In this case, light-induced renormalization is still observed (Fig. 3l; see more detailed analysis in Extended Data Fig. 3). The observation of similar light-induced renormalization even when direct optical transition is forbidden indicates that it is not caused by charge depletion but rather by Floquet band engineering.

## Pseudospin-selective Floquet engineering

The light-induced Floquet band engineering presented above is based on TrARPES data measured along the AC direction, with pump polarization also along the AC direction. To check whether there is any lattice-symmetry-enforced pseudospin selectivity, we show TrARPES dispersions measured at four different experimental geometries in Fig. 4 (see corresponding experimental geometry in Extended Data Fig. 1). Figure 4a,c shows a comparison of TrARPES dispersion images measured with AC pump polarization, and the scattering geometries are *s-pol.* and *p-pol.*, respectively. Although a stronger sideband is observed for *p-pol.* pump in Fig. 4c owing to the interference between Floquet states and Volkov states ('Floquet–Volkov states'[32]), the light-induced band renormalization is observed not only for the *p-pol.* pump scattering geometry but also for the *s-pol.* pump polarization, in which there is no contribution from Volkov states, suggesting that it is independent of the Volkov states (see a summary of the comparison in Extended Data Fig. 4). This suggests that the light-induced band renormalization is a fundamental feature to distinguish the Floquet band engineering from the emergence of pure Volkov states, because Volkov states do not renormalize the electronic structure of the host quantum materials, whereas the Floquet engineering does. Furthermore, a comparison of Fig. 4a,c and Fig. 4b,d shows that, when the pump polarization changes from AC pump to ZZ pump, the renormalization is strongly reduced, and the VB dispersion is similar to the equilibrium state (Fig. 4b,d). These results indicate that the light-induced band renormalization is intrinsically related to the pump polarization with respect to the crystal orientation, namely, there are lattice-symmetry-enforced pseudospin selection rules.

In the Floquet theory, the light–matter interaction renormalizes the electronic structures of black phosphorus and, therefore, the effect of Floquet band engineering is determined by the interaction matrix elements between electronic states with different Floquet indexed ($m$, $n$) bands. Theoretical analysis and calculation show that the VB edge with $m = 0$ and the CB edge with $n = -1$ are always coupled to open a hybridization gap for the AC pump, which becomes substantially reduced for the ZZ pump (see calculated results in Fig. 4e–h, Extended Data Fig. 5 and Supplementary Information). This is in good agreement with TrARPES experimental results and reflects the coupling of light with the pseudospin degree of freedom. Such pseudospin-selective Floquet band engineering is schematically summarized in Fig. 4i,j and analogous to the valley-selective Floquet band engineering proposed in monolayer $WS_2$ and $WSe_2$ (refs. [15,18,19]). Here we provide experimental signatures of Floquet band engineering in black phosphorus and show that the pseudospin can indeed play an important role through the light–matter interaction matrix elements (see Supplementary Information for more details).

## Near-resonance versus off-resonance pumping

The effects of light-induced band renormalization on near-resonance and off-resonance pumping are shown by changing the pump photon energy across the band gap, as schematically illustrated in Fig. 5a.

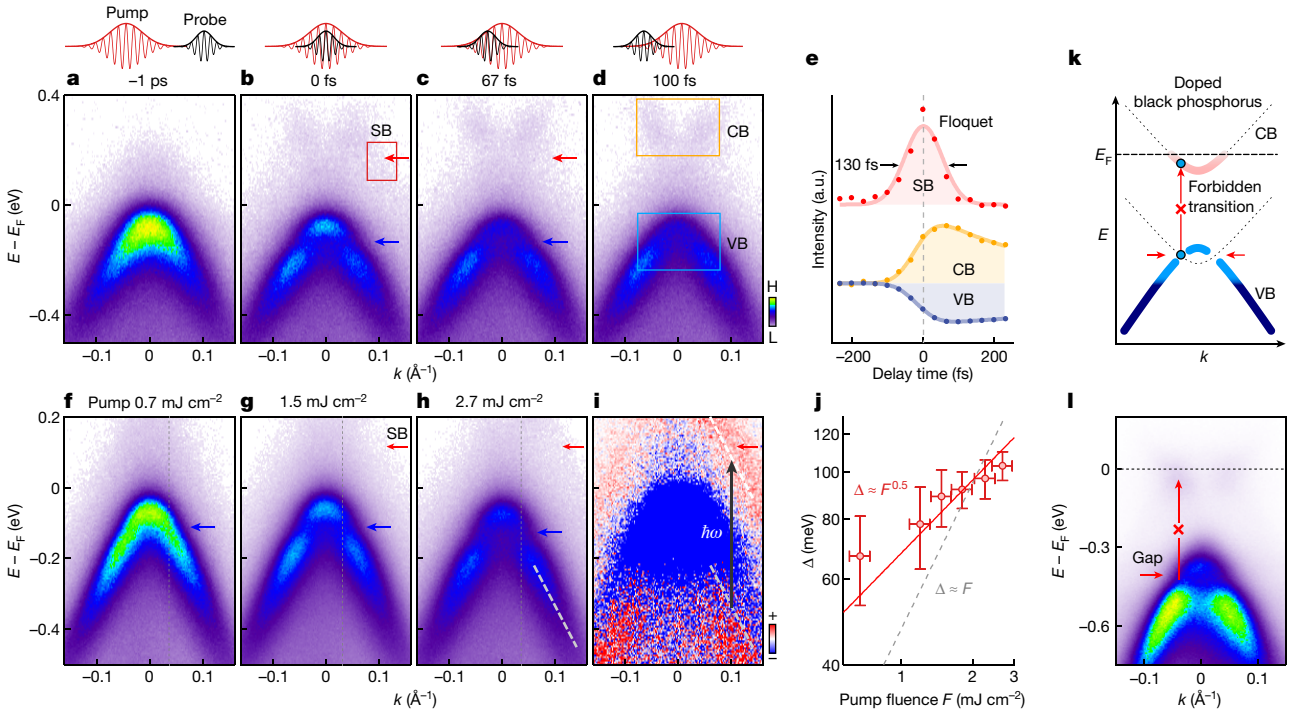


**Fig. 3 | Supporting evidence of Floquet band engineering. a**–**d**, TrARPES dispersion images measured at different delay times along the AC direction. The pump photon energy is 420 meV and the pump fluence is 2.3 mJ cm$^{-2}$. The pump polarization is parallel to the AC direction. The blue and red arrows point to the hybridization gap and Floquet sideband, respectively. **e**, Intensity of the Floquet sideband (integrated over the red box in **b**), CB and VB (integrated over the orange and blue boxes in **d**) as a function of delay time. **f**–**h**, TrARPES dispersion images measured at $\Delta t = 0$ with increasing pump fluence. **i**, Differential image obtained by subtracting data taken at $\Delta t = -1$ ps from **h**. The grey and white lines are guides to the VB and Floquet sideband. **j**, Extracted hybridization gap as a function of the pump fluence. **k**, Schematic dispersion for Floquet gap opening of electron-doped black phosphorus on near-resonance pumping. **l**, TrARPES dispersion images measured at $\Delta t = 0$ in electron-doped black phosphorus with pump photon energy of 400 meV and pump fluence of 3 mJ cm$^{-2}$.

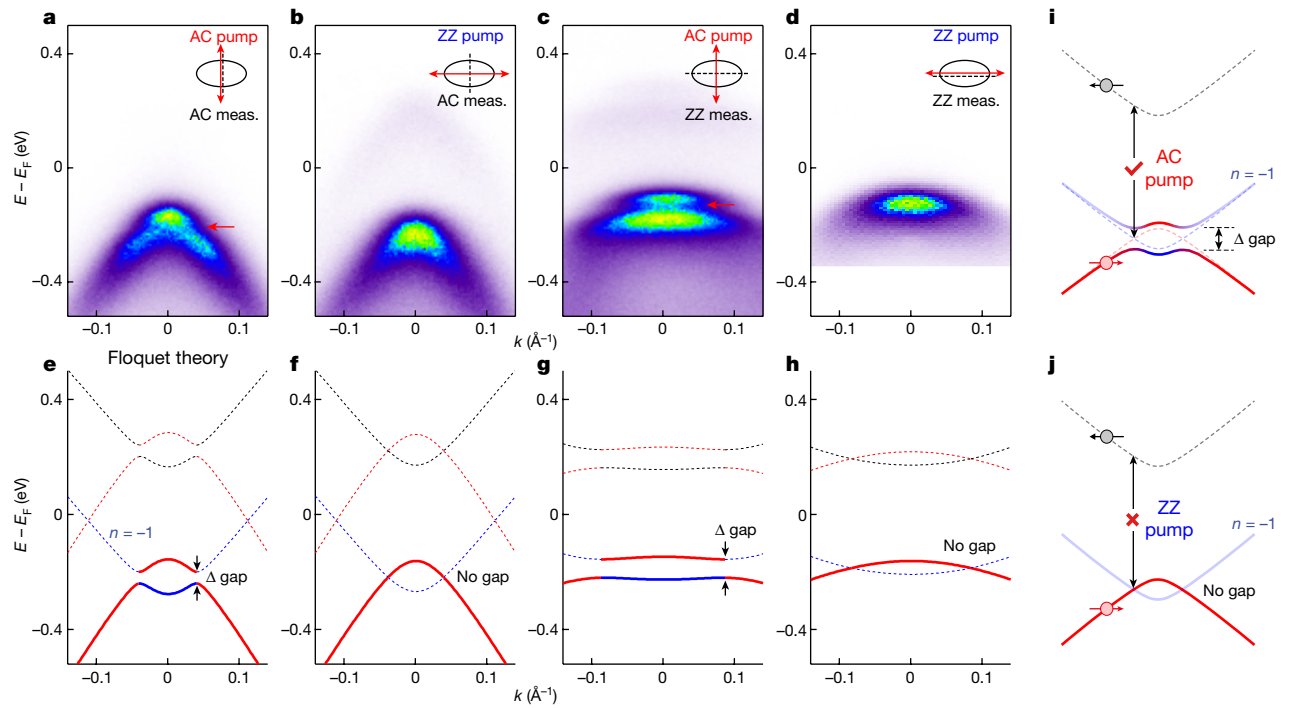


**Fig. 4 | Pseudospin-selective Floquet band engineering. a**–**d**, TrARPES dispersion images measured at $\Delta t = 0$ with combinations of different measurement directions and pump polarizations as schematically shown in the insets. The pump photon energy is 440 meV for **a** and **b** and 380 meV for **c** and **d**, and the pump fluence is 0.7 mJ cm$^{-2}$. **e**–**h**, Calculated Floquet band structures corresponding to **a**–**d**. **i**,**j**, Schematic summary of pseudospin-selective Floquet band engineering.

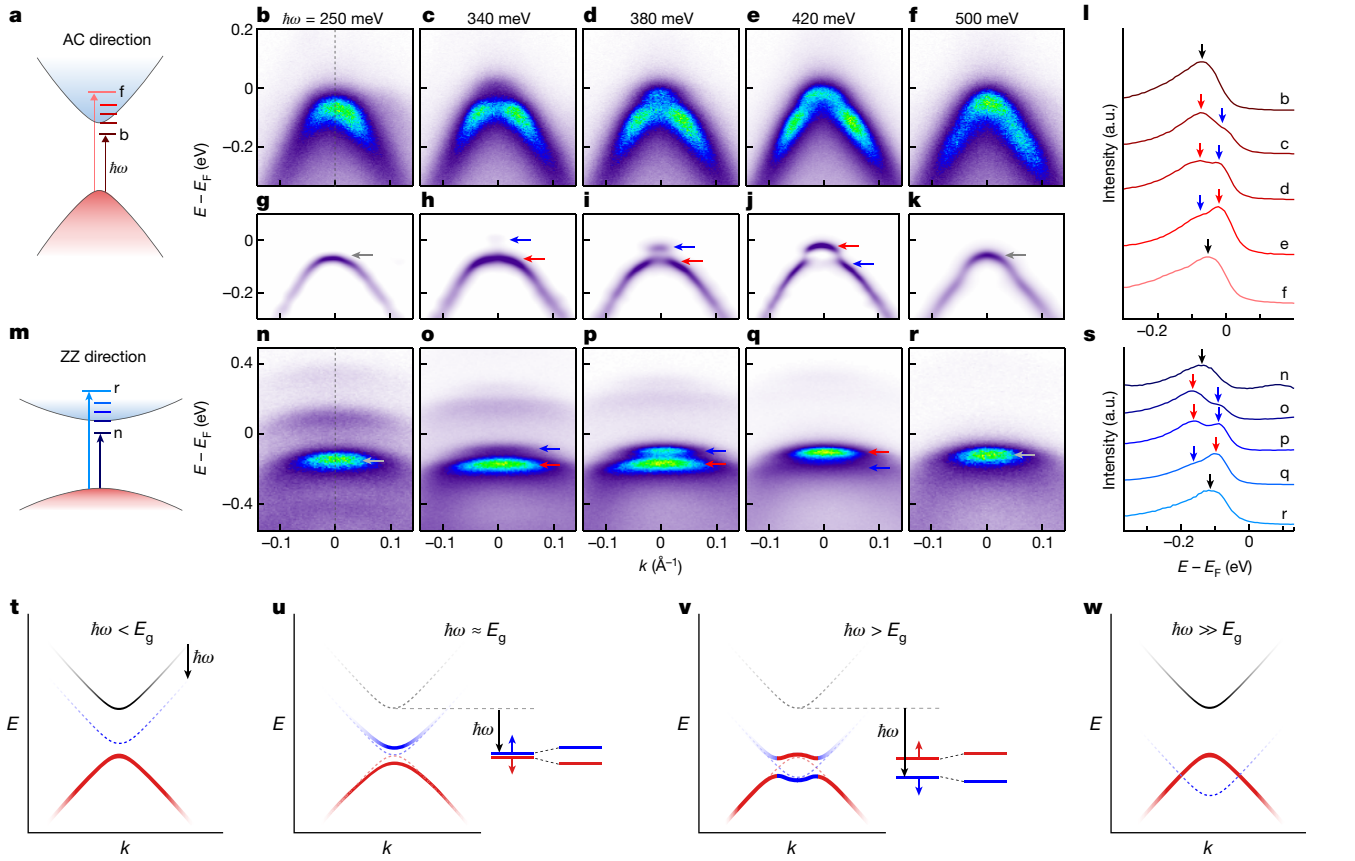


**Fig. 5 | Evolution of Floquet band engineering with pump photon energy.** **a**, A schematic for the band structure along the AC direction with various pump photon energies used. **b**–**k**, TrARPES dispersion images measured at $\Delta t = 0$ along the AC direction with different pump photon energies (**b**–**f**) and the corresponding second-derivative images (**g**–**k**). The pump polarization is along the AC direction of the sample and *s-pol*. with respect to the scattering plane and the pump fluence is 0.7 mJ cm$^{-2}$. **l**, EDCs at $k = 0$ for data shown in **b**–**f**. **m**, A schematic for the band structure along the ZZ direction and pump photon energies used. **n**–**r**, TrARPES dispersion images measured at $\Delta t = 0$ along the ZZ direction with different pump photon energies. The pump polarization is along the AC direction of the sample and *p-pol*. with respect to the scattering plane. The pump fluence is 0.7 mJ cm$^{-2}$. **s**, EDCs at $k = 0$ for data shown in **n**–**r**. **t**–**w**, A schematic summary of electronic structure on pumping at different photon energies. The insets in **u** and **v** show the energy shifts for the VB edge and the CB edge with $n = -1$.

Figure 5b–f shows dispersion images measured along the AC direction at different pump photon energies, and the corresponding second-derivative images are shown in Fig. 5g–k. A clear light-induced band renormalization is observed on pumping at photon energies from 340 meV to 420 meV (Fig. 5c–e), which are near resonance with the band gap of 330 meV. Furthermore, the transfer of spectral intensity from a stronger lower band to a stronger upper band (indicated by the arrows in Fig. 5h–j and EDCs at the Γ point in Fig. 5l) suggests a possible band inversion between the VB edge and the CB edge with $n = -1$ on increasing the pump photon energy. Notably, for off-resonance pumping, for example, 250 meV or 500 meV pump photon energy, the band renormalization is strongly reduced and becomes barely detectable experimentally (Fig. 5b,f,g,k). Similar pump-photon-energy-dependent light-induced band renormalization has also been observed for dispersions measured along the ZZ direction with AC pump polarization (see Fig. 5m–s). Although there is a stronger sideband owing to the Floquet–Volkov states in the *p-pol*. pump scattering geometry, the light-induced band renormalization is also observed on near-resonance pumping (Fig. 5o–q) and becomes strongly reduced for off-resonance pumping (Fig. 5n,r). Such pump-photon-energy-dependent light-induced band renormalization is also supported by theoretically calculated Floquet band structures based on the ab initio tight-binding Hamiltonian (see Extended Data Figs. 6 and 7 for a comparison between experimental results and calculated electronic structures).

Figure 5t–w shows a schematic summary of the pump-photon-energy-dependent Floquet band engineering. For below-gap excitation when the Floquet sideband is far away from the VB, no notable band renormalization is observed. Although high-order interaction ($|m - n| > 1$) can in principle also lead to light-induced band renormalization, the interaction strength is expected to be greatly reduced[1]. Increasing the pump photon energy to near resonance with the band gap, the CB edge with $n = -1$ approaches the VB edge, leading to marked renormalization, as schematically illustrated in Fig. 5u. Further increasing the pumpphoton energy so that the Floquet sideband overlaps with the VB, a hybridization gap occurs near the resonance points as schematically shown in Fig. 5v. At even higher pump photon energy, the band renormalization is reduced (Fig. 5w).

The light-induced band renormalization in black phosphorus is in line with the optical Stark effect[39], which is also strongly related to Floquet engineering. Although the optical Stark effect often involves atomic energy levels in atomic physics, Floquet band engineering refers to the dynamical momentum-dependent electronic structure hybridization between the Bloch band and Floquet sideband in the context of condensed matter physics. Here we resolve not only the energy shifts but also the momentum-dependent band renormalization. Such direct observation of Floquet band engineering in a layered quantum material provides the electronic structure counterpart of the optical Stark effect.

## Discussions and perspectives

The light-induced band renormalization of black phosphorus reported here distinguishes from previous Dirac materials[12,13] in two main aspects. First, although Floquet band engineering of $Bi_2Se_3$ and graphene does not depend on the crystal orientation owing to the overall isotropic electronic structure[12,32], the Floquet band engineering of black phosphorus exhibits a stronger pump polarization selectivity with respect to the crystal orientation, which is enforced by the lattice symmetry, thereby providing a control knob for turning on and off the Floquet band engineering through the pseudospin degree of freedom. Second, although Dirac fermions can couple to low-energy photons at different energies effectively owing to the conical dispersion, in semiconducting black phosphorus, in which the dispersion shows a parabolic behaviour near the gap edge, the interaction between the Bloch band and Floquet sideband is strongly enhanced on resonant pumping near the band gap.

Notably, resonance pumping of semiconductors has been conventionally thought of as activating more excitation and scattering channels, such as electron–electron and electron–phonon interactions, which might heat up the samples[19] and even destroy the Floquet states[27]. Our results show that the Floquet states survive within the duration of the pump pulse and the band renormalization is enhanced on near-resonance pumping, thereby highlighting the importance of resonance pumping in the Floquet band engineering of black phosphorus. Such pseudospin-selective Floquet band engineering offers an exciting opportunity to manipulate time-resolved optical response in black phosphorus by means of linear dichroic pumping near resonance. Finally, we expect that such a near-resonance pumping strategy can be applied to more quantum materials, paving a critical step towards the dynamical engineering of the transient electronic structures on the ultrafast timescale, as well as the experimental realization of exotic electronic states, such as the Floquet topological phases[3,8,10].

## Online content

Any methods, additional references, Nature Portfolio reporting summaries, source data, extended data, supplementary information, acknowledgements, peer review information; details of author contributions and competing interests; and statements of data and code availability are available at https://doi.org/10.1038/s41586-022-05610-3.


1. Oka, T. & Aoki, H. Photovoltaic Hall effect in graphene. *Phys. Rev. B* **79**, 081406(R) (2009).
2. Kitagawa, T., Oka, T., Brataas, A., Fu, L. & Demler, E. Transport properties of nonequilibrium systems under the application of light: photoinduced quantum Hall insulators without Landau levels. *Phys. Rev. B* **84**, 235108 (2011).
3. Lindner, N. H., Refael, G. & Galitski, V. Floquet topological insulator in semiconductor quantum wells. *Nat. Phys.* **7**, 490–495 (2011).
4. Jotzu, G. et al. Experimental realization of the topological Haldane model with ultracold fermions. *Nature* **515**, 237–240 (2014).
5. Rechtsman, M. C. et al. Photonic Floquet topological insulators. *Nature* **496**, 196–200 (2013).
6. Shirley, J. H. Solution of the Schrödinger equation with a Hamiltonian periodic in time. *Phys. Rev.* **138**, B979 (1965).
7. Oka, T. & Kitamura, S. Floquet engineering of quantum materials. *Annu. Rev. Condens. Matter Phys.* **10**, 387–408 (2019).
8. Rudner, M. S. & Lindner, N. H. Band structure engineering and non-equilibrium dynamics in Floquet topological insulators. *Nat. Rev. Phys.* **2**, 229–244 (2020).
9. Weber, C. P. Ultrafast investigation and control of Dirac and Weyl semimetals. *J. Appl. Phys.* **129**, 070901 (2021).
10. de la Torre, A. et al. *Colloquium*: Nonthermal pathways to ultrafast control in quantum materials. *Rev. Mod. Phys.* **93**, 041002 (2021).
11. Bao, C., Tang, P., Sun, D. & Zhou, S. Light-induced emergent phenomena in 2D materials and topological materials. *Nat. Rev. Phys.* **4**, 33–48 (2021).
12. Wang, Y., Steinberg, H., Jarillo-Herrero, P. & Gedik, N. Observation of Floquet-Bloch states on the surface of a topological insulator. *Science* **342**, 453–457 (2013).
13. McIver, J. W. et al. Light-induced anomalous Hall effect in graphene. *Nat. Phys.* **16**, 38–41 (2020).
14. Kim, J. et al. Ultrafast generation of pseudo-magnetic field for valley excitons in $WSe_2$ monolayers. *Science* **346**, 1205–1208 (2014).
15. Sie, E. J. et al. Valley-selective optical Stark effect in monolayer $WS_2$. *Nat. Mater.* **14**, 290–294 (2015).
16. Shan, J.-Y. et al. Giant modulation of optical nonlinearity by Floquet engineering. *Nature* **600**, 235–239 (2021).
17. Katan, Y. T. & Podolsky, D. Modulated Floquet topological insulators. *Phys. Rev. Lett.* **110**, 016802 (2013).
18. De Giovannini, U., Hübener, H. & Rubio, A. Monitoring electron-photon dressing in $WSe_2$. *Nano Lett.* **16**, 7993–7998 (2016).
19. Claassen, M., Jia, C., Moritz, B. & Devereaux, T. P. All-optical materials design of chiral edge modes in transition-metal dichalcogenides. *Nat. Commun.* **7**, 13074 (2016).
20. Zhang, X.-X., Ong, T. T. & Nagaosa, N. Theory of photoinduced Floquet Weyl semimetal phases. *Phys. Rev. B* **94**, 235137 (2016).
21. Ashcroft, N. W. & Mermin, N. D. *Solid State Physics* (Saunders College, 1976).
22. Hübener, H., Sentef, M. A., De Giovannini, U., Kemper, A. F. & Rubio, A. Creating stable Floquet–Weyl semimetals by laser-driving of 3D Dirac materials. *Nat. Commun.* **8**, 13940 (2017).
23. Chan, C.-K., Oh, Y.-T., Han, J. H. & Lee, P. A. Type-II Weyl cone transitions in driven semimetals. *Phys. Rev. B* **94**, 121106(R) (2016).
24. Yan, Z. & Wang, Z. Tunable Weyl points in periodically driven nodal line semimetals. *Phys. Rev. Lett.* **117**, 087402 (2016).
25. Chan, C.-K., Lee, P. A., Burch, K. S., Han, J. H. & Ran, Y. When chiral photons meet chiral fermions: photoinduced anomalous Hall effects in Weyl semimetals. *Phys. Rev. Lett.* **116**, 026805 (2016).
26. Park, S. et al. Steady Floquet–Andreev states in graphene Josephson junctions. *Nature* **603**, 421–426 (2022).
27. Aeschlimann, S. et al. Survival of Floquet–Bloch states in the presence of scattering. *Nano Lett.* **21**, 5028–5035 (2021).
28. Jung, S. W. et al. Black phosphorus as a bipolar pseudospin semiconductor. *Nat. Mater.* **19**, 277–281 (2020).
29. Tran, V., Soklaski, R., Liang, Y. & Yang, L. Layer-controlled band gap and anisotropic excitons in few-layer black phosphorus. *Phys. Rev. B* **89**, 235319 (2014).
30. Qiao, J., Kong, X., Hu, Z. X., Yang, F. & Ji, W. High-mobility transport anisotropy and linear dichroism in few-layer black phosphorus. *Nat. Commun.* **5**, 4475 (2014).
31. Yuan, H. et al. Polarization-sensitive broadband photodetector using a black phosphorus vertical p–n junction. *Nat. Nanotechnol.* **10**, 707–713 (2015).
32. Mahmood, F. et al. Selective scattering between Floquet–Bloch and Volkov states in a topological insulator. *Nat. Phys.* **12**, 306–310 (2016).
33. Nurmamat, M. et al. Prolonged photo-carriers generated in a massive-and-anisotropic Dirac material. *Sci. Rep.* **8**, 9073 (2018).
34. Chen, Z. et al. Band gap renormalization, carrier multiplication, and Stark broadening in photoexcited black phosphorus. *Nano Lett.* **19**, 488–493 (2018).
35. Roth, S. et al. Photocarrier-induced band-gap renormalization and ultrafast charge dynamics in black phosphorus. *2D Mater.* **6**, 031001 (2019).
36. Chen, Z. et al. Spectroscopy of buried states in black phosphorus with surface doping. *2D Mater.* **7**, 035027 (2020).
37. Hedayat, H. et al. Non-equilibrium band broadening, gap renormalization and band inversion in black phosphorus. *2D Mater.* **8**, 025020 (2021).
38. Kremer, G. et al. Ultrafast dynamics of the surface photovoltage in potassium-doped black phosphorus. *Phys. Rev. B* **104**, 035125 (2021).
39. Autler, S. H. & Townes, C. H. Stark effect in rapidly varying fields. *Phys. Rev.* **100**, 703 (1955).

# Methods

### Sample preparation and electron doping

Black phosphorus single crystals were grown by the chemical vapour transport method. A mixture of red phosphorus lump (Alfa Aesar, 99.999%), tin grains (Aladdin, ≥ 99.5%) and iodine crystals (Alfa Aesar, 99.9%) was sealed under vacuum in a silica tube. The tube was heated to 400 °C within 2 h and maintained at 400 °C for 2 h, then heated to 600 °C and maintained at 600 °C for 1 day. The tube was slowly cooled to 350 °C from 600 °C at a cooling rate of 10 °C $h^{-1}$ and then furnace-cooled to room temperature. Millimetre-size, high-quality black phosphorus single crystals were obtained.

The samples were cleaved and measured at a temperature of 80 K in an ultrahigh-vacuum chamber with a base pressure better than $5 \times 10^{-11}$ torr. The electron-doped black phosphorus is obtained by in situ deposition of Cs using a commercial dispenser (SAES). The dispenser was operated at a current of 4.7 A and the distance between the sample and the source was about 13 cm. The dispersion is monitored by in situ ARPES measurements until sufficient electron doping was reached.

### TrARPES measurements

TrARPES measurements were performed in the home laboratory at Tsinghua University with a regenerative amplifier laser with centre wavelength at 800 nm and 10 kHz repetition rate. The pulse energy is 1.3 mJ and most of the beam (80%) is used to drive the optical parametric amplifier. The MIR pulses are produced by non-collinear differential frequency generation using the signal and idle of the optical parametric amplifier. The probe beam with photon energy of 6.2 eV is generated by a three-step fourth harmonics generation process using beta barium borate crystals. For electron-doped sample, there is an overall shift of the electronic structure induced by surface photovoltaic effect with a long relaxation timescale[36–38] and the Fermi energy is obtained by the Fermi–Dirac fitting to the spectrum before pump.

The pump and probe beams are almost collinear, with a similar incident angle of $\theta = 54°$ as shown in Extended Data Fig. 1a. Four different experimental geometries with different pump polarizations and measurement directions are shown in Extended Data Fig. 1. The typical pump fluence of 0.7 mJ $cm^{-2}$ used by *s-pol.* pump corresponds to an electric field strength of $6.8 \times 10^7$ V $m^{-1}$. This is calculated from the pump fluence $F$ by $E = t_s\sqrt{2\frac{F}{\tau}\sqrt{\frac{\mu_0}{\epsilon_0}}}$, in which $t_s$ is the Fresnel transmission coefficient ($t_s = 0.29$ for the incident angle of 54°, calculated from the reflectance in ref. [31] using the method from ref. [12]) and $\tau$ is the estimated pump pulse duration (90 fs).

For the penetration depth of the pump and probe beams in TrARPES measurements, the penetration depth of MIR pump light (for example, 400 meV) is estimated to be 14 nm from the optical absorbance of 4% per layer[29], which is much larger than the probing depth of 3.5 ± 2 nm by the 6.2-eV probe laser estimated from the universal curve[40]. Therefore the probed beam examines an overall uniformly illuminated region. For electron-doped sample by deposition of Cs, the depth of electron doping in black phosphorus is estimated to be 15 nm at 80 K (ref. [37]), which is much larger than the ARPES probing depth. Therefore TrARPES signals on electron-doped sample are dominated by the electron-doped region near the surface.

A convenient method to directly visualize the dispersion is to extract the peak positions by taking the second derivative of the dispersion image, for example, Fig. 2c,d. Here a modified second derivative (or 2D curvature) is applied,

$$\nabla^2 I_{\mathrm{ARPES}} = \frac{\partial^2 I_{\mathrm{ARPES}}}{\partial x^2} + \frac{\partial^2 I_{\mathrm{ARPES}}}{\partial y^2}$$

Considering the different units of $k$ and $E$ by taking a transformation for $x$ and $y$, this becomes

$$C(x,y) \approx \frac{\left[1 + C_x\left(\frac{\partial f}{\partial x}\right)^2\right]C_y\frac{\partial^2 f}{\partial y^2} - 2C_xC_y\frac{\partial f}{\partial x}\frac{\partial f}{\partial y}\frac{\partial^2 f}{\partial x \partial y} + \left[1 + C_y\left(\frac{\partial f}{\partial y}\right)^2\right]C_x\frac{\partial^2 f}{\partial x^2}}{\left[1 + C_x\left(\frac{\partial f}{\partial y}\right)^2 + C_y\left(\frac{\partial f}{\partial y}\right)^2\right]^{3/2}}$$

Such a method has been widely applied in the ARPES data analysis for a direct visualization of ARPES dispersions. For quantitative analysis, the dispersion is extracted by fitting the peak positions in EDCs (see, for example, Fig. 2g,h).

### More pump-fluence-dependent TrARPES data and analysis

More pump-fluence-dependent TrARPES dispersion images are shown in Extended Data Fig. 2a–f. Clear gap opening is observed at high pump fluence (as indicated by the blue arrows). The size of the hybridization gap is extracted from the zoom-in EDCs at the resonance momentum positions shown in Extended Data Fig. 2h–m and the extracted values are plotted in Extended Data Fig. 2n as a function of pump fluence. The extracted light-induced gap shows a scaling of $\Delta \propto F^{0.5}$ with the pump fluence $F$, supporting the Floquet engineering interpretation of the light-induced band renormalization.

### Exclusion of an alternative explanation based on charge depletion

To check if charge depletion can explain our experimental results, TrARPES measurements are performed on in situ electron-doped sample, so that the CB and VB near the band edges are both below the Fermi energy. The fact that these states are both occupied means that optical transition on near-resonance pumping is forbidden.

A comparison of near-resonance pumping on undoped sample (Extended Data Fig. 3a–f) versus doped sample (Extended Data Fig. 3g–l) shows that, although optical transition is blocked in electron-doped black phosphorus (see schematic illustration in Extended Data Fig. 3g), the light-induced gap is still clearly observed (Extended Data Fig. 3i–l), thereby indicating that the light-induced gap is not related to charge depletion on optical absorption. Therefore the observation of similar light-induced renormalization on near-resonance pumping, regardless of when direct optical transition is allowed or forbidden, indicates that it is not caused by charge depletion but rather by the Floquet band engineering.

### Comparison of experimental results for AC pump with different scattering geometries

The pump polarization with respect to the scattering plane (*p-pol.* or *s-pol.*) can lead to selective excitation of Floquet–Volkov states versus pure Floquet states[32]. For black phosphorus, the sideband shows a stronger intensity for *p-pol.* pump owing to Floquet–Volkov states and a weaker intensity for *s-pol.* pump owing to pure Floquet states, which is consistent with reported results on $Bi_2Se_3$ (ref. [32]). Notably, the band renormalization (indicated by the red arrows in Extended Data Fig. 4) and sideband are observed for both *p-pol.* and *s-pol.* pump scattering geometries, similar to the case of $Bi_2Se_3$, suggesting that the light-induced band renormalization is a more intrinsic effect of Floquet engineering than the sideband intensity. Such band renormalization is important evidence to distinguish the Floquet band engineering from simply the emergence of Volkov states, because Volkov states do not renormalize the electronic structure of the host quantum materials, whereas the Floquet engineering does.

### Pump-polarization-dependent Floquet band engineering using the tight-binding calculation and $\mathbf{k}\cdot\mathbf{p}$ model

Through the analysis of the tight-binding calculation and the Floquet $\mathbf{k}\cdot\mathbf{p}$ Hamiltonian around the Γ point (see more details in the Supplementary Information), we find that the pseudospin selection rules in the equilibrium electronic state in black phosphorus, which are constrained by

the lattice symmetry, strongly influence its hybridization gaps in the Floquet electronic structures. A large hybridization gap is observed along both the AC and ZZ directions only for the AC pump, as shown in Extended Data Fig. 5.

### Pump-photon-energy-dependent Floquet band engineering and theoretical calculations

The dispersions for different pump photon energies are calculated for dispersions along both the AC (Extended Data Fig. 6) and ZZ (Extended Data Fig. 7) directions from the ab initio tight-binding calculations within the Floquet theory, which are in good overall agreement with the TrARPES dispersions measured at $\Delta t = 0$. The hybridization gap is maximum on near-resonance pumping.

### First-principles calculation

We performed the density functional theory (DFT) to calculate the electronic structure of black phosphorus without the laser pumping by using the Vienna Ab initio Simulation Package (VASP)[41].

The projector-augmented wave potentials[42] were used and the cut-off of plane-wave energy was set as 400 eV, and the Γ-centred $k$-mesh was sampled as $12 \times 12 \times 12$ in the Brillouin zone (BZ) of the primitive cell (see Extended Data Fig. 8a–c). The convergence condition of an electronic self-consistent loop was $10^{-6}$ eV and the force criterion was set as 0.01 eV Å$^{-1}$. The van der Waals corrections[43,44] were included for both lattice relaxation and electronic self-consistent calculations. We used the Perdew–Burke–Ernzerhof type exchange-correlation functional[45] to obtain the optimized lattice structures. For the calculation of electronic state, we used the Heyd–Scuseria–Ernzerhof hybrid functional[46] to obtain the direct band gap as 330 meV at the Z point, which is consistent with our ARPES experimental observations. By using the wannier90[47–49], we constructed the tight-binding Hamiltonian $\hat{H}^{\mathrm{TB}}(\mathbf{r}, \mathbf{k})$ from the ab initio calculations (see Extended Data Fig. 8d–f).

### Floquet Hamiltonian

We apply the Floquet theory to calculate the band structures of black phosphorus under the laser pumping. In our TrARPES experiments, the linear polarized probe pulse is used with a duration of 100 fs, which roughly corresponded to ten optical cycles of pump pulse. In the calculations, we assume that the non-equilibrium Floquet band could be formed in a few optical cycles, which is confirmed by previous calculations through time-dependent DFT[18]. Therefore the Floquet theory is a good approximation to study the laser-pumping effect in this case. Herein we use the Peierls substitution to include the influence of light field and obtain the time-dependent tight-binding Hamiltonian as

$$\hat{H}^{\mathrm{TB}}(\mathbf{k}) \to \hat{H}^{\mathrm{TB}}\left(\mathbf{k} + \frac{\mathrm{e}}{\hbar}\mathbf{A}(t)\right) \tag{1}$$

in which $\mathbf{A}(t) = (A_0 \sin\Omega t, 0, 0)$ or $(0, A_0 \sin\Omega t, 0)$ is the vector potential of pump light and $\Omega$ is its frequency. So the evolution of the wavefunction $\Psi_\alpha(t)$ in the black phosphorus satisfies the time-dependent Schrödinger equation

$$\hat{H}^{\mathrm{TB}}(\mathbf{k}, t)|\Psi_\alpha(t)\rangle = \mathrm{i}\frac{\partial}{\partial t}|\Psi_\alpha(t)\rangle \tag{2}$$

From the Floquet theorem, we could expand $\Psi_\alpha(t)$ in the Floquet basis $|\Phi_\mathrm{i}(t)\rangle$ so that it satisfies

$$\begin{aligned} |\Phi_\alpha(t+T)\rangle &= |\Phi_\alpha(t)\rangle \\ |\Psi_\alpha(t)\rangle &= \mathrm{e}^{-\mathrm{i}\epsilon_\alpha t}|\Phi_\alpha(t)\rangle \end{aligned} \tag{3}$$

in which $\epsilon_\alpha$ are known as Floquet quasienergies and $T = \frac{2\pi}{\Omega}$. Then we expand $|\Phi_\alpha(t)\rangle$ by a complete set of $\{|u_\alpha^m\rangle\}$

$$|\Phi_\alpha(t)\rangle = \sum_m \mathrm{e}^{-\mathrm{i}m\Omega t}|u_\alpha^m\rangle \tag{4}$$

Substituting equations (3) and (4) into equation (2), we get

$$\sum_m \hat{H}^{\mathrm{TB}}(\mathbf{k}, t)\mathrm{e}^{-\mathrm{i}m\Omega t}|u_\alpha^m\rangle = \sum_m [\epsilon_\alpha + m\Omega]\mathrm{e}^{-\mathrm{i}m\Omega t}|u_\alpha^m\rangle \tag{5}$$

Finally we integrate against $\mathrm{e}^{\mathrm{i}n\Omega t}$ on both sides of the above equation and obtain

$$\sum_m \frac{1}{T}\int_0^T \mathrm{d}t\hat{H}^{\mathrm{TB}}(\mathbf{k}, t)\mathrm{e}^{\mathrm{i}(n-m)\Omega t}|u_\alpha^m\rangle = [\epsilon_\alpha + n\Omega]\ |u_\alpha^n\rangle \tag{6}$$

Let $\hat{H}^{\mathrm{FTB}}_{n,m}(\mathbf{k}) = \frac{1}{T}\int_0^T \mathrm{d}t\hat{H}^{\mathrm{TB}}(\mathbf{k}, t)\mathrm{e}^{\mathrm{i}(n-m)\Omega t} - m\Omega\delta_{mn}$, then finally we get the Floquet tight-binding Hamiltonian that satisfies the equation

$$\sum_m \hat{H}^{\mathrm{FTB}}_{n,m}(\mathbf{k})|u_\alpha^m\rangle = \epsilon_\alpha|u_\alpha^n\rangle \tag{7}$$

The index $\alpha$ labels eigenstates and $m$ and $n$ are the Fourier mode indices. Here the time-dependent Schrödinger equation is mapped to a time-independent eigenvalue problem in an extended Hilbert space. The Floquet Hamiltonian $\hat{H}^{\mathrm{FTB}}(\mathbf{k})$ can be written as a block matrix

$$\hat{H}^{\mathrm{FTB}}(\mathbf{k}) = \begin{bmatrix} \ddots & \vdots & \vdots & \vdots & \iddots \\ \cdots & H^{\mathrm{FTB}}_{-1,-1}(\mathbf{k}) + \Omega I & H^{\mathrm{FTB}}_{-1,0}(\mathbf{k}) & H^{\mathrm{FTB}}_{-1,1}(\mathbf{k}) & \cdots \\ \cdots & H^{\mathrm{FTB}}_{0,-1}(\mathbf{k}) & H^{\mathrm{FTB}}_{0,0}(\mathbf{k}) & H^{\mathrm{FTB}}_{0,1}(\mathbf{k}) & \cdots \\ \cdots & H^{\mathrm{FTB}}_{1,-1}(\mathbf{k}) & H^{\mathrm{FTB}}_{1,0}(\mathbf{k}) & H^{\mathrm{FTB}}_{1,1}(\mathbf{k}) - \Omega I & \cdots \\ \iddots & \vdots & \vdots & \vdots & \ddots \end{bmatrix} \tag{8}$$

We can diagonalize $\hat{H}^{\mathrm{FTB}}(\mathbf{k})$ to obtain the Floquet band structure of the black phosphorus. The electric field of $6.8 \times 10^7$ V m$^{-1}$ is used to calculate the TrARPES spectra.

## Data availability

The data that support the findings of this study are available from the corresponding author on request.


40. Seah, M. P. & Dench, W. Quantitative electron spectroscopy of surfaces: a standard data base for electron inelastic mean free paths in solids. *Surf. Interface Anal.* **1**, 2–11 (1979).
41. Kresse, G. & Furthmüller, J. Efficient iterative schemes for ab initio total-energy calculations using a plane-wave basis set. *Phys. Rev. B* **54**, 11169 (1996).
42. Kresse, G. & Joubert, D. From ultrasoft pseudopotentials to the projector augmented-wave method. *Phys. Rev. B* **59**, 1758 (1999).
43. Dion, M., Rydberg, H., Schröder, E., Langreth, D. C. & Lundqvist, B. I. Van der Waals density functional for general geometries. *Phys. Rev. Lett.* **92**, 246401 (2004).
44. Klimeš, J., Bowler, D. R. & Michaelides, A. Van der Waals density functionals applied to solids. *Phys. Rev. B* **83**, 195131 (2011).
45. Perdew, J. P., Burke, K. & Ernzerhof, M. Generalized gradient approximation made simple. *Phys. Rev. Lett.* **77**, 3865 (1996).
46. Krukau, A. V., Vydrov, O. A., Izmaylov, A. F. & Scuseria, G. E. Influence of the exchange screening parameter on the performance of screened hybrid functionals. *J. Chem. Phys.* **125**, 224106 (2006).
47. Mostofi, A. A. et al. wannier90: a tool for obtaining maximally-localised Wannier functions. *Comput. Phys. Commun.* **178**, 685–699 (2008).
48. Mostofi, A. A. et al. An updated version of wannier90: a tool for obtaining maximally-localised Wannier functions. *Comput. Phys. Commun.* **185**, 2309–2310 (2014).
49. Marzari, N., Mostofi, A. A., Yates, J. R., Souza, I. & Vanderbilt, D. Maximally localized Wannier functions: theory and applications. *Rev. Mod. Phys.* **84**, 1419 (2012).


**Acknowledgements** We thank N.L. Wang, R.-B. Liu, D. Sun and Y.H. Wang for useful discussions. This work is supported by the National Key R&D Program of China (grant no. 2021YFA1400100), the National Natural Science Foundation of China (grant nos. 11725418, 12234011 and 11427903) and National Key R&D Program of China (grant nos. 2020YFA0308800 and 2016YFA0301004). P.Y. and W.D. acknowledge the support of the Basic Science Center

Project of NSFC (grant no. 51788104). S.M. acknowledges supports from Ministry of Science and Technology (grant no. 2021YFA1400201), National Natural Science Foundation of China (grant no. 12025407) and Chinese Academy of Sciences (grant no. YSBR047).

**Author contributions** Shuyun Z. conceived the research project. Shaohua Z., C.B., Q.G., Haoyuan Z. and T.L. performed the TrARPES measurements and analysed the data. Haoyuan Z. grew the black phosphorus single crystal. B.F., Hui Z., H.L., P.T., S.M. and W.D. performed the theoretical analysis and calculation, and the results shown in the manuscript are by B.F., P.T. and W.D. C.B., Shaohua Z. and Shuyun Z. wrote the manuscript, and all authors contributed to the discussions and commented on the manuscript.

**Competing interests** The authors declare no competing interests.

**Additional information**

**Supplementary information** The online version contains supplementary material available at https://doi.org/10.1038/s41586-022-05610-3.

**Correspondence and requests for materials** should be addressed to Shuyun Zhou.

**Peer review information** *Nature* thanks the anonymous reviewers for their contribution to the peer review of this work.

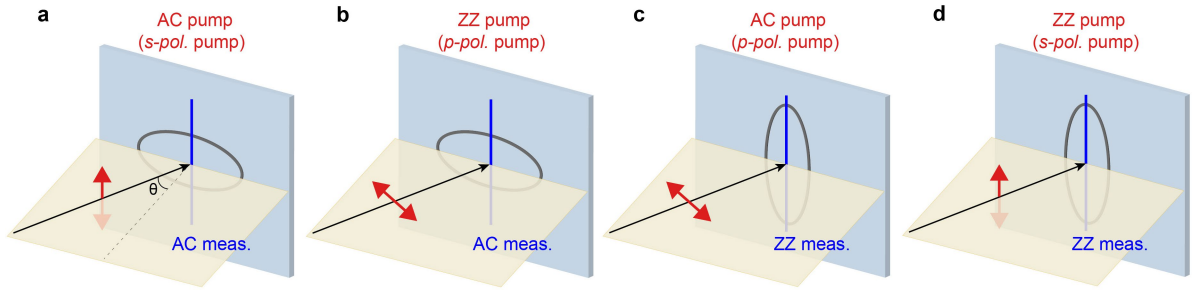


**Extended Data Fig. 1 | Experimental geometries of TrARPES measurements.** **a**–**d**, Schematics for four different combinations of pump polarizations and measurement directions along the AC or ZZ directions. The blue line indicates the ARPES measurement direction and the red arrow represents the pump polarization. The black ellipses represent the anisotropic electronic pocket of black phosphorus.

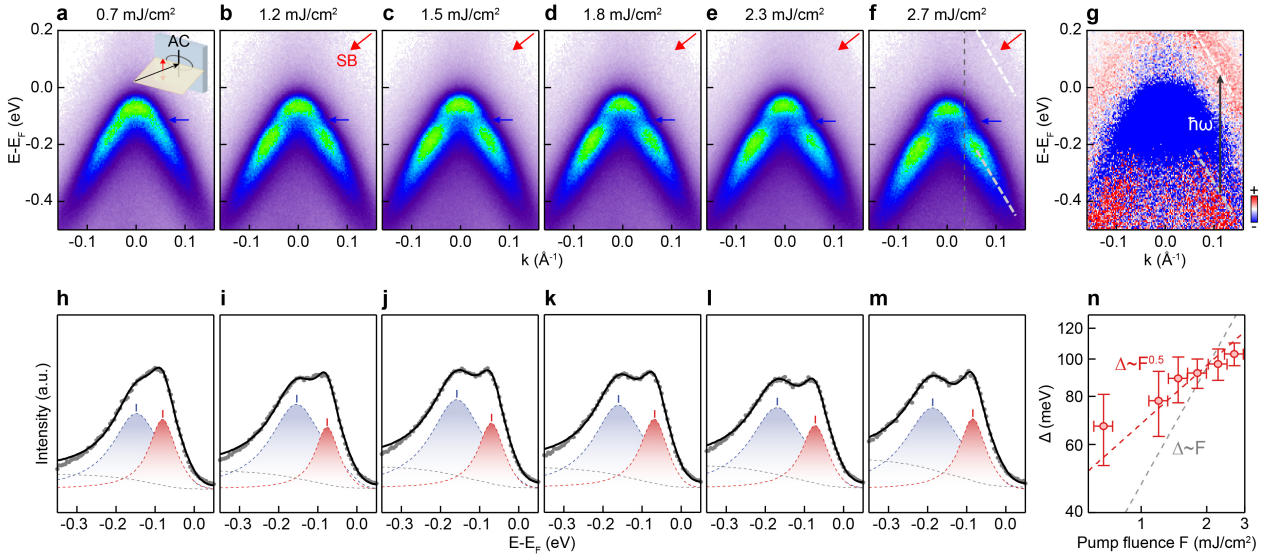


**Extended Data Fig. 2 | Pump-fluence-dependent hybridization gap and observation of Floquet sidebands. a**–**f**, TrARPES dispersions along the AC direction with different pump fluences (*s-pol*. pump, $\hbar\omega = 420$ meV, $\Delta t = 0$). The red and blue arrows point to the Floquet sideband of the VB and hybridization gap. **g**, The differential TrARPES dispersion with a pump fluence of 2.7 mJ cm$^{-2}$ after subtracting the dispersion before pump. **h**–**m**, EDCs for data shown in **a**–**f** at the momentum point of the hybridization gap (dashed line in **f**) and fitting curves. **n**, The extracted hybridization gap as a function of pump fluence. The error bar of the hybridization gap is defined as the upper limit when the energy position is clearly offset from the peak in **h**–**m** and the error bar of the pump fluence is defined by the fluctuation of pump power (10%).

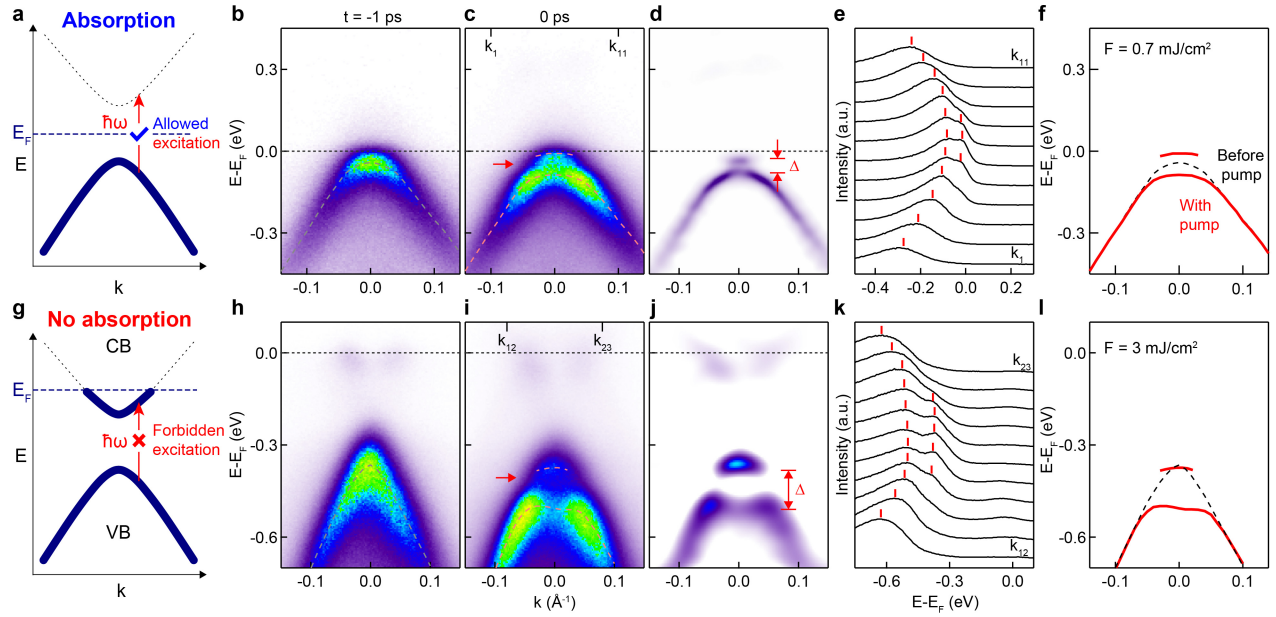


**Extended Data Fig. 3 | Undoped sample versus electron-doped sample (forbidden optical absorption) on near-resonance pumping. a**, Schematic illustration of the electronic structure of undoped black phosphorus with unoccupied CB. Direct optical transition from VB to CB is allowed on near-resonance pumping. **b**,**c**, TrARPES dispersion images measured in undoped sample along the AC direction at $\Delta t = -1$ ps (**b**) and $\Delta t = 0$ (**c**). The pump beam is polarized along the AC direction with photon energy of 380 meV and the pump fluence is 0.7 mJ cm$^{-2}$. **d**,**e**, Second-derivative image and EDCs of TrARPES data shown in **c**. **f**, Extracted dispersions before pump (dashed black curve) and with pump (red curves). **g**, Schematic illustration of the electronic structure of electron-doped black phosphorus with occupied CB edge. Direct optical transition from VB to CB is forbidden on near-resonance pumping. **h**–**l**, Similar results as **b**–**f** but in electron-doped sample using pump pulses with photon energy of 400 meV and pump fluence of 3 mJ cm$^{-2}$. The Fermi energy is obtained by the Fermi–Dirac fitting to the spectrum of electron-doped black phosphorus before pump ($\Delta t = -1$ ps).

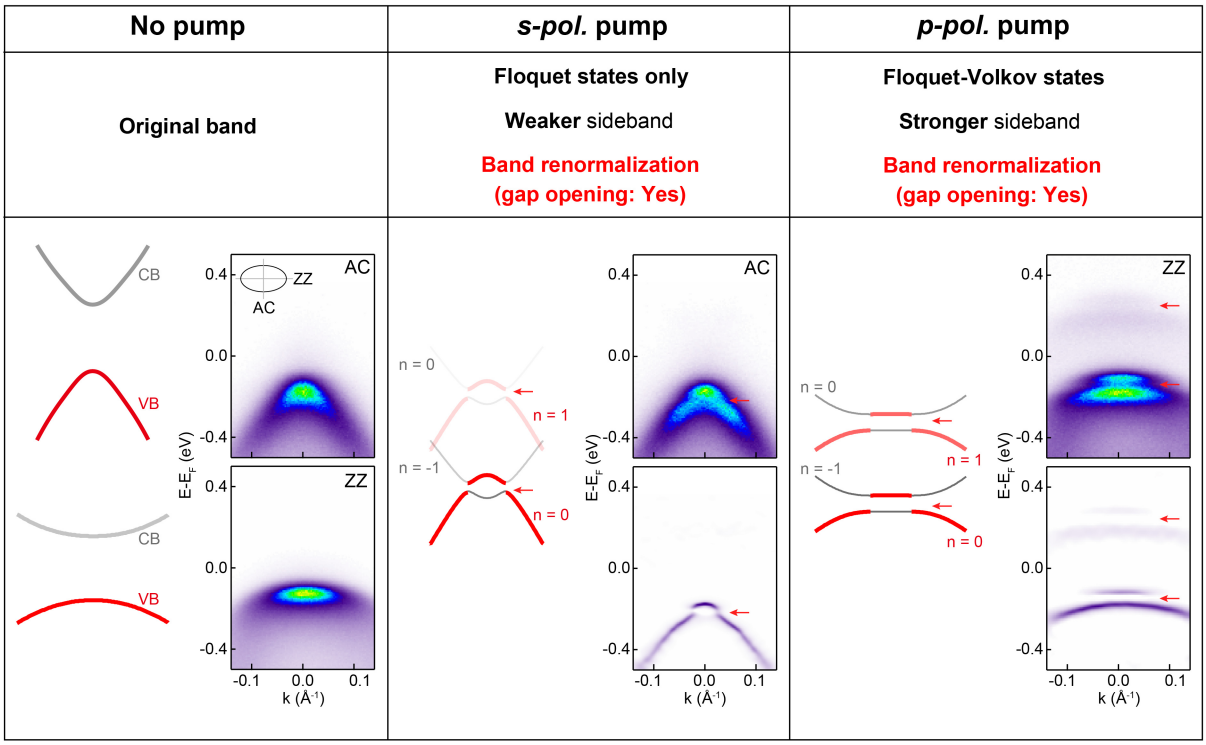


**Extended Data Fig. 4 | Summary of Floquet band engineering for black phosphorus for *s-pol.* pump and *p-pol.* pump when the pump polarization is parallel to the AC direction.** The pump photon energy is 440 and 380 meV for *s-pol.* and *p-pol.* pump, respectively. The pump fluence is 0.7 mJ cm$^{-2}$.

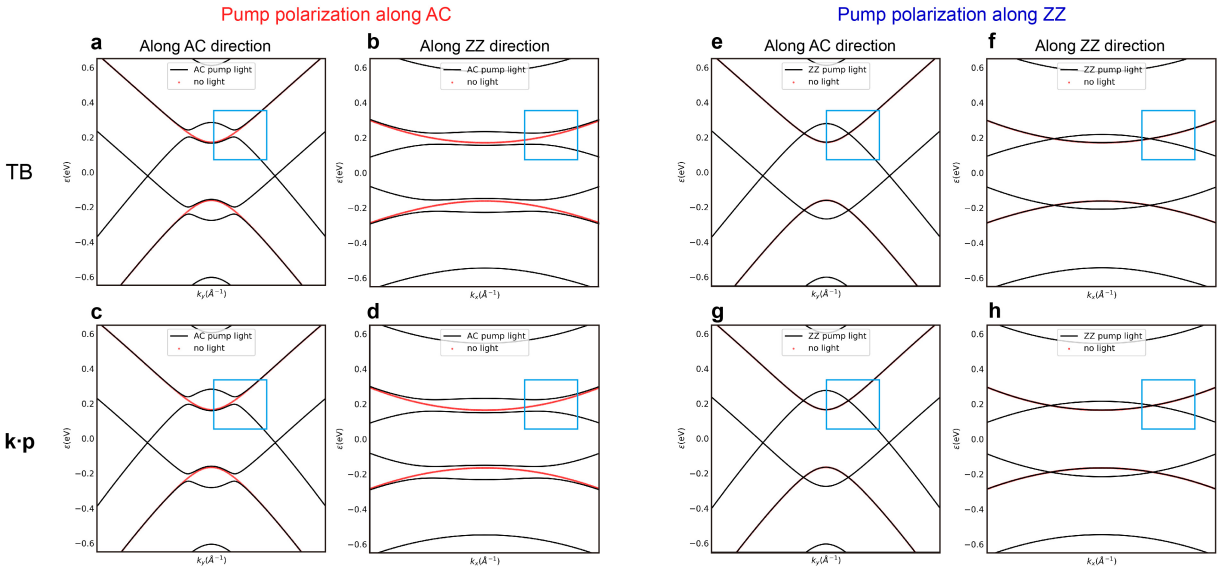


**Extended Data Fig. 5 | Theoretical calculation of Floquet band structure. a–d**, Floquet band structure with AC pump for dispersions along the AC and ZZ directions using the tight-binding model (**a**,**b**) and the **k · p** model (**c**,**d**). **e–h**, Similar results as **a–d** but with ZZ pump.

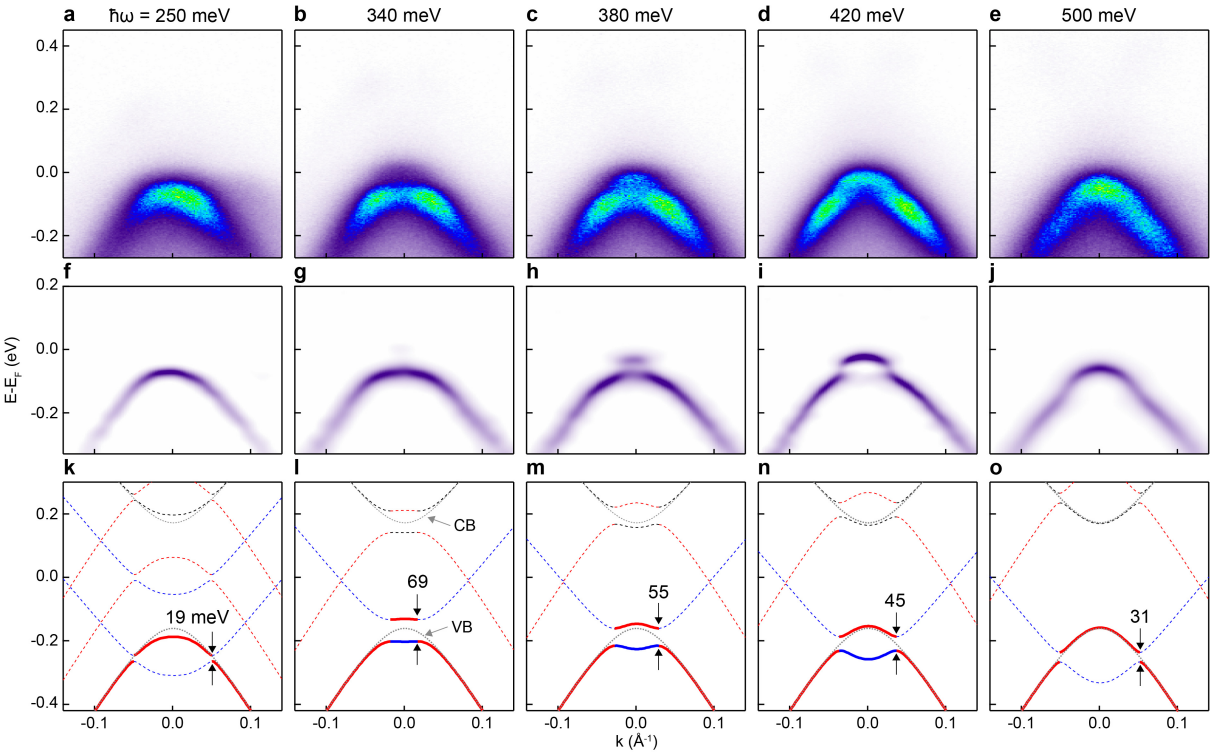


**Extended Data Fig. 6 | Comparison of experimental and theoretical dispersions along the AC direction for TrARPES with different pump photon energies. a–j**, TrARPES dispersions along the AC direction (**a–e**) and corresponding second-derivative images (**f–j**) with different pump photon energies at a pump fluence of 0.7 mJ cm$^{-2}$. **k–o**, Calculated Floquet band structures obtained from the ab initio tight-binding calculations with the Floquet theory to compare with **a–e**. The dotted black curves show the dispersions for the VB and the CB in the equilibrium state for comparison.

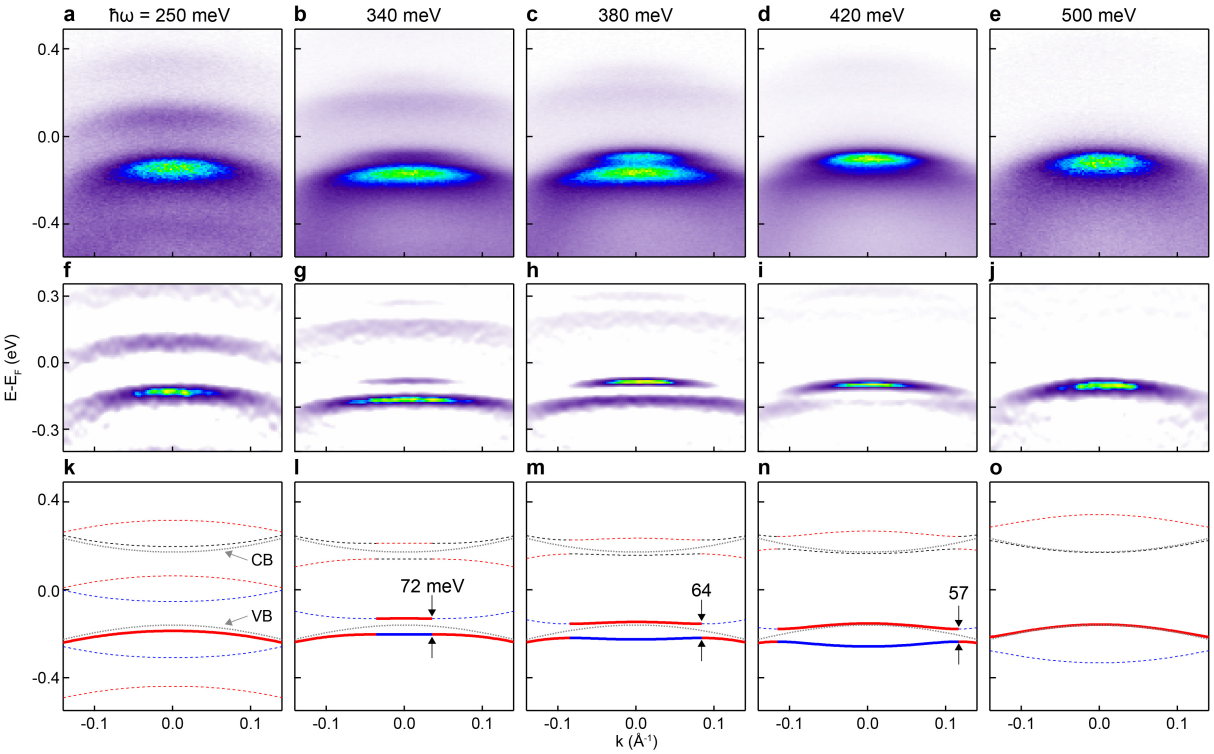


**Extended Data Fig. 7 | Comparison of experimental and theoretical dispersions along the ZZ direction for TrARPES with different pump photon energies. a–j**, TrARPES dispersions along the ZZ direction (**a**–**e**) and corresponding second-derivative images (**f**–**j**) with different pump photon energies at a pump fluence of 0.7 mJ cm$^{-2}$. **k**–**o**, Calculated Floquet band structures obtained from the ab initio tight-binding calculations with the Floquet theory to compare with **a**–**e**. The dotted black curves show the dispersions for the VB and the CB in the equilibrium state for comparison.

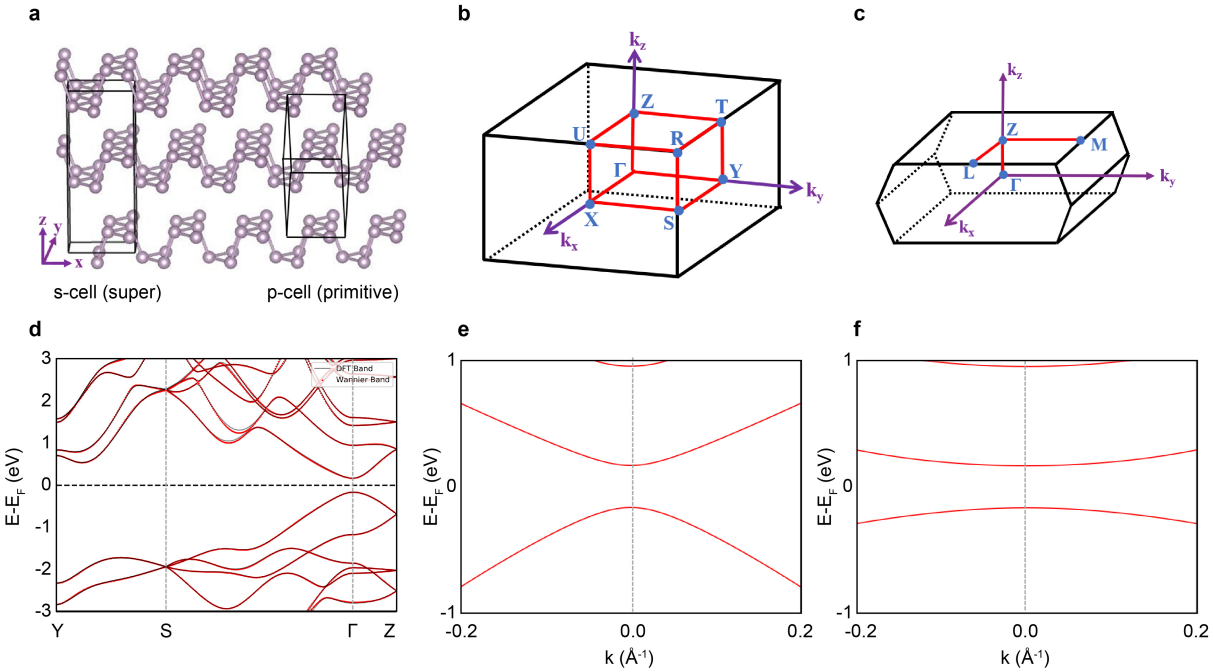


**Extended Data Fig. 8 | Atomic and electronic structure of black phosphorus. a**, Atomic structure of black phosphorus. The primitive cell of four atoms is on the right and the supercell of eight atoms is on the left. **b**, The BZ of the supercell. **c**, The BZ of the primitive cell. **d**, Comparison of the calculated band structures from DFT calculations and tight-binding calculations along high symmetry lines in the reduced BZ of the supercell. **e**,**f**, The calculated band structure around the Γ point along the AC direction (**e**) and along the ZZ direction (**f**). The Fermi level is set as zero.